Nano Res (2009) 2: 857–864
DOI 10.1007/s12274-009-9084-x
Research Article

Water-Controlled Synthesis of Low-Dimensional Molecular Crystals and the Fabrication of a New Water and Moisture Indicator

Zhuoyu Ji[1,2], Huanli Dong[1], Ming Liu[2] (✉), and Wenping Hu[1] (✉)

[1] Beijing National Laboratory for Molecular Sciences, Key Laboratory of Organic Solids, Institute of Chemistry, Chinese Academy of Sciences, Beijing 100190, China

[2] Key Laboratory of Nano-Fabrication and Novel Devices Integrated Technology, Institute of Microelectronics, Chinese Academy of Sciences, Beijing 100029, China

Received: 8 July 2009 / Revised: 13 August 2009 / Accepted: 25 August 2009

ABSTRACT

Arrays of low-dimensional molecular crystals of square columns (1-D) and nanolamellae (2-D) of $Zn[TCNQ]_2(H_2O)_2$ with large areas (up to 10–20 cm^2) have been synthesized by controlled addition of water to Zn and TCNQ. Based on the ability to accurately control the reaction, a new moisture and water indicator has been developed. The simple method, the large areas of material prepared, the fine size tuning, and the typical semiconductor behavior of the resulting low-dimensional molecular materials promise applications in molecular electronics as well as nanoelectronics. The system is an effective indicator for the detection of traces of water and moisture.

KEYWORDS

Molecular materials, molecular crystals, nanomaterials, water indicator

Molecular materials with interesting electrical, optical, and magnetic properties are a key subset of organic solids. "Hybrid" materials are of particular interest because they combine two or more properties not traditionally present in the same material, such as the combination of electrical/magnetic metal centers and conducting organic systems, i.e., metal–organic framework molecular materials. These exhibit not only intriguing architectures but also unexpected properties in asymmetric catalysis, magnetism, photoluminescence, memory, switching and so on. Moreover, materials where the metal ions bind to bi- or multi-dentate organic ligands by coordinate bonding may be synthesized from simple subunits by rapid and efficient self-assembly.

Since the first report by Dupont in the 1960s [1–10], molecular materials of metal–organic frameworks based on 7,7,8,8-tetracyanoquinodimethane (TCNQ) have undergone a significant growth and expansion, including the development of charge-transfer complexes based on Cu and Ag [11–15]. In contrast to the abundance of investigations of the TCNQ complexes of Cu and Ag [11–15], research into to charge-transfer complexes of other transition metals

Address correspondence to Ming Liu, liuming@ime.ac.cn; Wenping Hu, huwp@iccas.ac.cn

is still relatively underdeveloped [16–19]. Here we introduce a simple way for the controlled synthesis of low-dimensional $Zn[TCNQ]_2(H_2O)_2$ based on the fine control of the addition of water to Zn and TCNQ. A new moisture and water indicator has also been developed utilizing the color change during the synthesis of $Zn[TCNQ]_2(H_2O)_2$.

The controlled synthesis of $Zn[TCNQ]_2(H_2O)_2$ is depicted in Fig. 1(a). First, Zn substrates were immersed into TCNQ/CH_3CN solution and then one or several drops of water were added to the solution. In the absence of water, no reaction took place between Zn and TCNQ. However, as soon as water was dropped into the TCNQ solution, dark blue products were formed on the Zn substrates (Fig. 1(b)). By means of this simple controlled synthesis, products with areas varying from several mm^2 up to as large as 10–20 cm^2 could be produced. This facile method for the synthesis of molecular crystals with such large areas is an attractive way of preparing materials for application in molecular electronics.

It is interesting that the morphologies of the final products varied with the reaction time. Products with two morphologies were observed, square columns and nanolamellae, as shown in Figs. 2(a) and 2(b). The chemical composition of the columns and lamellae was determined through energy-dispersive X-ray analysis (EDX). The EDX profiles of the columns and nanolamellae exhibited similar characteristics (see Fig. S-1 in the Electronic Supplementary Material (ESM)); the peaks of C, N, O, and Zn elements were clearly identified, confirming that the products were $Zn[TCNQ]_x$-based materials. Figure 2(c) shows a typical transmission electron microscopy (TEM) image of a square column and its corresponding selected area electron diffraction (SAED) pattern (Fig. 2(d)). The same pattern was observed for different parts of the column, indicating that the whole column was a single crystal. Similarly, the single crystal nature of the lamellae was demonstrated, as shown in Figs. 2(e) and 2(f).

X-ray photoelectron spectroscopy (XPS) data (see Fig. S-2 in the ESM) of the sub-micro columns were characterized by Zn $2P_{3/2}$ and Zn $2P_{1/2}$ peaks, with the positions of the peaks at 1023.2 eV and 1046.4 eV suggesting that the products contained Zn^{2+} ions [20]. Meanwhile, the N 1s peak appeared as a single feature at 399.05 eV, which is indicative of the presence of only one type of TCNQ [11, 21, 22]. The Fourier transform infrared (FT-IR) spectrum of the square columns is shown in Fig. 3(a). The band at 2196 cm^{-1} occurs at lower energy than that of the

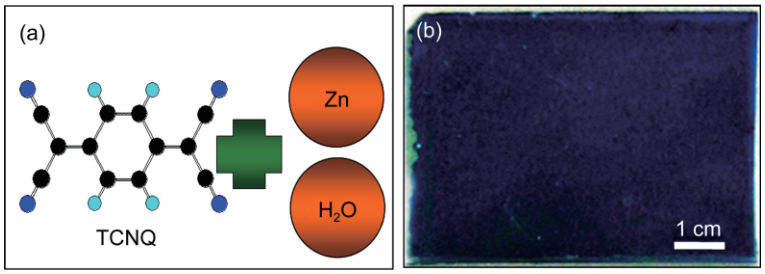

Figure 1 (a) Schematic diagram illustrating the controlled synthesis of the charge transfer complex $Zn[TCNQ]_2(H_2O)_x$ by addition of water. (b) Controlled synthesis affords the dark blue product $Zn[TCNQ]_2(H_2O)_x$ with large areas of up to 10–20 cm^2

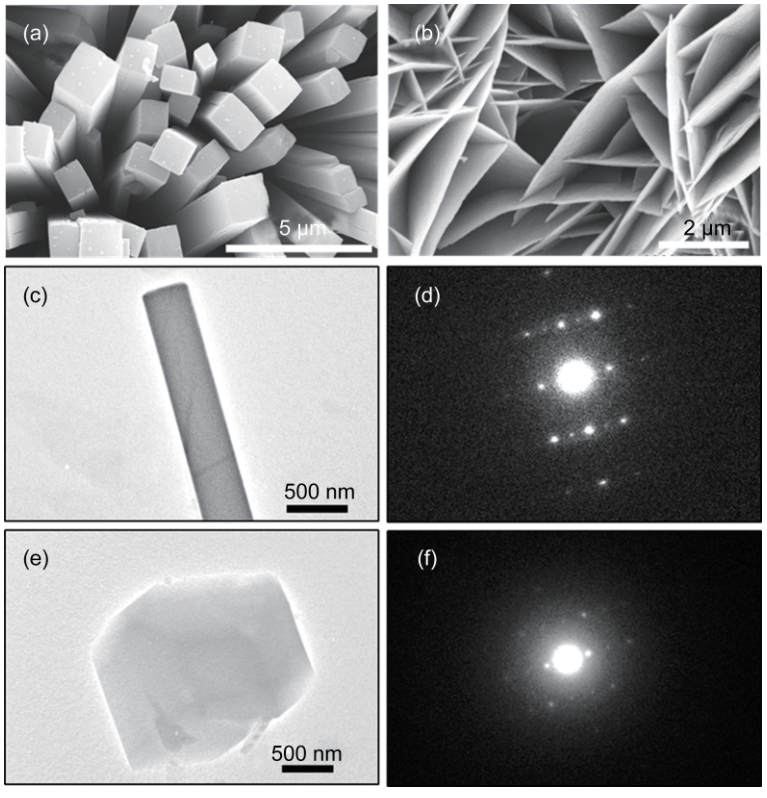

Figure 2 (a) Square columns and (b) nanolamellae of the $Zn[TCNQ]_x$-based material. (c, e) TEM images and (d, f) SAED patterns of an individual column and lamella of the $Zn[TCNQ]_x$-based material

infrared (IR) band of neutral TCNQ at 2224 cm^{-1}, and is characteristic of the C≡N stretching mode, indicating the existence of the reduced $[TCNQ]^-$ radical [23]. The sharp peak at 1507 cm^{-1} is further evidence of the presence of the reduced $[TCNQ]^-$ radical [18, 24]. The distinct δ(C–H) peak at 823–824 cm^{-1} indicates the presence of $[TCNQ]^-$ rather than the $[TCNQ–TCNQ]^-$ σ-dimer. The broad IR absorption band at 3440 cm^{-1}, along with a weak band at ~1630 cm^{-1} indicate the presence of coordinated water molecules. The IR data strongly suggest that the products are the hydrated $Zn[TCNQ]_2(H_2O)_2$ phase. The presence of two water molecules was further confirmed by the thermogravity analysis (TGA) data (see Fig. S-3 in the ESM). The columns lost ~7% of their mass at temperatures below 225 °C, while the lamellae lost ~7% of their mass at temperatures below 260 °C, which corresponds to the loss of two water molecules. At higher temperatures, a large change in mass occurred, indicative of decomposition *via* loss of TCNQ, as previously observed with $M[TCNQ]_2(H_2O)_2$ complexes [19, 24]. The distinct difference in the TGA traces of the columns and lamellae possibly indicates that they are different phases. A careful analysis of the FT-IR spectra of the columns and lamellae was carried out in the fingerprint region 2100–2300 cm^{-1}.

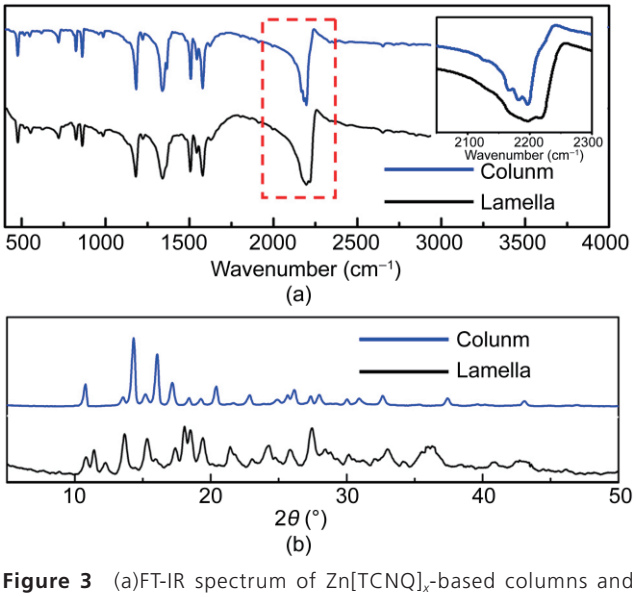

Figure 3 (a)FT-IR spectrum of $Zn[TCNQ]_x$-based columns and nanolamellae (inset: the fingerprint area of 2100–2300 cm^{-1}). (b) XRD patterns of $Zn[TCNQ]_x$-based columns and nanolamellae. FT-IR spectra were recorded by using pressed pellets of the mixture of the columns and KBr, and XRD patterns were obtained by using powdered $Zn[TCNQ]_2(H_2O)_x$

The columns exhibited typical peaks at 2196, 2178, and 2167 cm^{-1}, while the peaks for the lamellae were located at 2219 and 2178 cm^{-1} (Inset in Fig. 3(a)), confirming the different phases of the columns and lamellae. Moreover, the different powder X-ray diffraction patterns (Fig. 3(b)) of the columns and lamellae confirmed that the columns and nanolamellae are different phases. The UV-visible absorption spectrum of the columns showed a peak at ~392 nm that can be attributed to neutral $Zn[TCNQ]_2(H_2O)_2$, and peaks at 745 nm and 843 nm that can be assigned to the TCNQ anion radical of $Zn(TCNQ)_2(H_2O)_2$ [25–28] (see Fig. S-4 in the ESM). Thus, the synthesis of $Zn(TCNQ)_2(H_2O)_2$ can be depicted by the reaction

$$Zn + 2TCNQ + 2H_2O \longrightarrow Zn(TCNQ)_2(H_2O)_2$$

It was found that the column phase formed quickly after the zinc plate was placed into the mixed solution, while the formation of the lamellae needed much a longer time, suggesting that the columns are the kinetically favored phase I, and the lamellae are the thermodynamically favored phase II.

The two phases of $Zn[TCNQ]_2(H_2O)_2$ are very similar to those of another charge transfer complex, CuTCNQ. However, in the formation of CuTCNQ, only Cu and TCNQ solution are involved and the reaction is difficult to control due to the rapid reaction between copper and TCNQ. In contrast, the formation of $Zn[TCNQ]_2(H_2O)_2$ involves a ternary system, since in the absence of water no reaction takes place between Zn and TCNQ. Hence, by controlling the amount of water, the reaction between Zn and TCNQ can be finely controlled. Using limited amounts of water restricts the generation of new $Zn[TCNQ]_2(H_2O)_2$ allowing the phase transformation to the thermodynamic product to take place. Based on such fine control of the reaction, square columns and nanolamellae could be obtained with large areas (see Fig. S-5 in the ESM). The transformation from square columns to nanolamellae is vividly depicted in Fig. 4. The transformation first occurs on the surface of the columns, and hence at the beginning of the transformation, the whole surface of the columns becomes covered with the nanolamellae, forming a hybrid of 1-D and 2-D structures.

Because the growth of the square columns and nanolamellae is based on the accurate control of

the reaction between Zn and TCNQ by addition of water, the size of the micro and nanometer sized crystals of $Zn[TCNQ]_2(H_2O)_2$ can be finely tuned. For example, the width of the square columns was varied from ~100 nm to several micrometers (Figs. 5(a) and 5(b)). Similarly, the thickness of the lamellae could be tuned from ~20–30 nm to ~100–200 nm (Figs. 5(c) and 5(d)). This ability to fine tune the size of 1-D and 2-D nanostructures of molecular materials by the control of reaction conditions is attractive in terms of applications of the materials in nanoelectronics. Although nanoelectronics has attracted worldwide attention and undergone rapid development, despite thousands of nanostructures and particles having been synthesized and applied in electronics, it is still a great challenge to control the size and patterning of nanostructures. Here, we have demonstrated a simple method to achieve such control by employing a ternary reaction system.

The formation mechanism of the square columns of $Zn[TCNQ]_2(H_2O)_2$ is different from that of the square columns of the charge transfer complex CuTCNQ. For CuTCNQ, the formation process of its columns can be depicted by a "coalescence" mechanism. The primary product is always the kinetic product of nanorods, and the nanorods tend to aggregate with each other, so that they quickly evolve into "square columns" with widths of several hundreds of nanometers [29]. However, for $Zn[TCNQ]_2(H_2O)_2$ the primary products seem to be amorphous square columns (see Fig. S-6 in the ESM) which subsequently evolve into crystalline square columns.

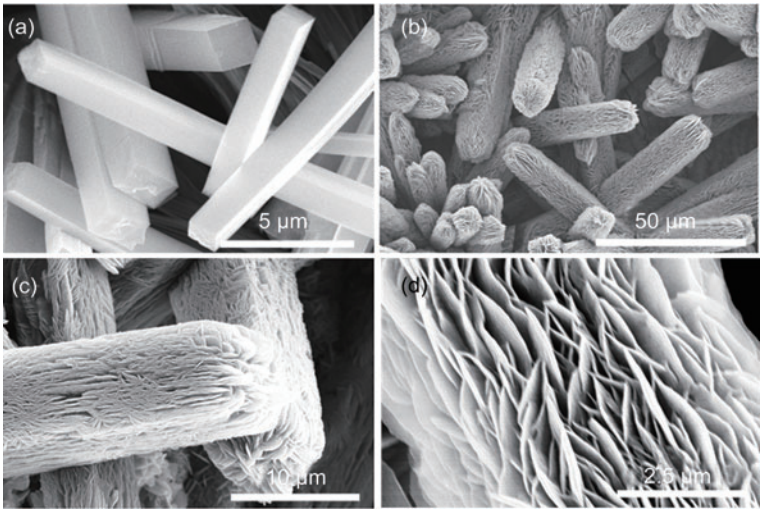

Figure 4 (a) Square columns of $Zn[TCNQ]_2(H_2O)_2$. (b) The transformation of square columns to nanolamellae giving a hybrid of 1-D and 2-D structures (c, d) Enlarged SEM images showing the transformation of square columns to nanolamellae

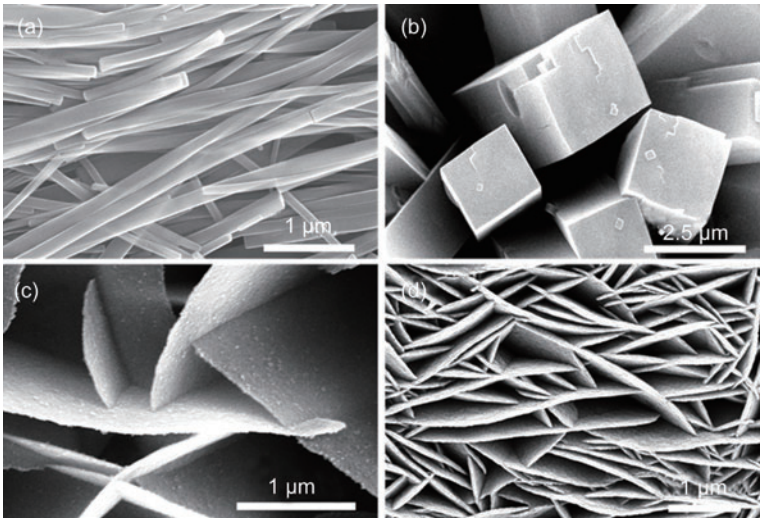

Figure 5 (a) Square columns with diameter around ~100 nm. (b) Square columns with diameter around ~2–5 μm. (c) Lamellae with thickness around ~20–30 nm. (d) Lamellae with thickness around ~100–200 nm

It is important to understand the electrical properties of molecular crystals because of their potential application in devices. A series of devices based on an individual single crystalline column of $Zn[TCNQ]_2(H_2O)_2$ were fabricated with a coplanar electrode geometry. Single crystalline square columns were employed because single crystals of a molecular material are better able to reveal the intrinsic properties of the material and open up prospects for the fabrication of high quality devices. A schematic diagram of the device fabrication process is given in the top left inset of Fig. 6. First, an individual $Zn[TCNQ]_2(H_2O)_2$ column was moved onto a Si/SiO_2 (300 nm) substrate by mechanical probes [30]. Second, a micro Au wire was used as the mask for the deposition of Au electrodes on the crystal by thermal evaporation (as shown in the top left inset of Fig. 6). With this method a gap of ~20 μm was produced between the two electrodes (as shown in the bottom right inset of Fig. 6). A typical current voltage (I–V) plot of the

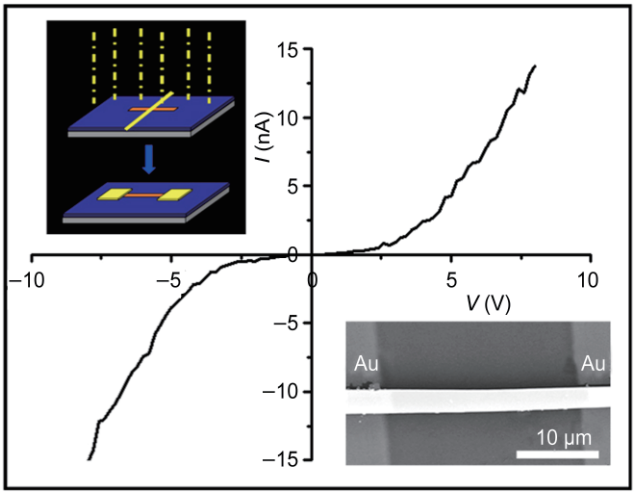

Figure 6 *I–V* characteristics of a single column. The insets show a schematic illustration of the device fabrication process and the SEM image of an individual column device

single crystalline column is shown in Fig. 6. The highly reproducible, symmetrical *I–V* characteristics of the devices suggest symmetrical contacts between the column and electrodes. Two separate voltage regions were observed, with a nearly ohmic *I–V* dependence at low voltage and a rough $I–V^2$ dependence at higher voltages, indicating a space charge limited current (SCLC) in the crystal [31]. Moreover, it is interesting to note that all the devices exhibited similar semiconductor behavior, and even when higher voltages were applied to the devices until they broke, no switching phenomena were observed. The *I–V* characteristics of the nanolamellae were similar to those of the square columns. Therefore, it is reasonable to conclude that $Zn[TCNQ]_2(H_2O)_2$ is not a switching material, in contrast to CuTCNQ which shows high resistance under low voltage bias ("OFF" state) and high conductivity under high voltage bias ("ON" state). However, the typical semiconductor behavior of the single crystalline products of square columns and nanolamellae suggested potential applications of the 1-D and 2-D nanostructures of $Zn[TCNQ]_2(H_2O)_2$.

An important application of $Zn[TCNQ]_2(H_2O)_2$ is based on the characteristic of its water-controlled synthesis. Traces of water will result in the generation of the dark blue molecular material. Hence, the appearance of the dark blue $Zn[TCNQ]_2(H_2O)_2$, i.e., the color change of the Zn substrate, can be used as an indicator to monitor the appearance of water, such as in inspection of traces of water or leak hunting. As preliminary experimental results, the dependence between the color of the Zn substrate and the amount of water in the reaction of Zn and TCNQ to give $Zn[TCNQ]_2(H_2O)_2$ is depicted in Fig. 7(a). When different amounts of water were added to the TCNQ solution, the colours of the substrates were tuned because of the generation of $Zn[TCNQ]_2(H_2O)_2$ on the substrates. Without water added to the solution, no products appear. Hence, the appearance of $Zn[TCNQ]_2(H_2O)_2$ can be used as an effective indicator of the presence of traces of water.

The appearance of $Zn[TCNQ]_2(H_2O)_2$ can also be used as an indicator to monitor the presence of moisture. With different amounts of moisture, the amount of $Zn[TCNQ]_2(H_2O)_2$ generated on the substrates will be different, and consequently the colors of substrates will be tuned. Simple color observation can be used to monitor the amount of moisture. For example, it was found that the colors of co-deposited films of TCNQ:Zn (5:1) (50 nm), or films produced by alternate deposition of Zn (1 nm)/TCNQ (5 nm) (with 10 repetitions), varied with moisture

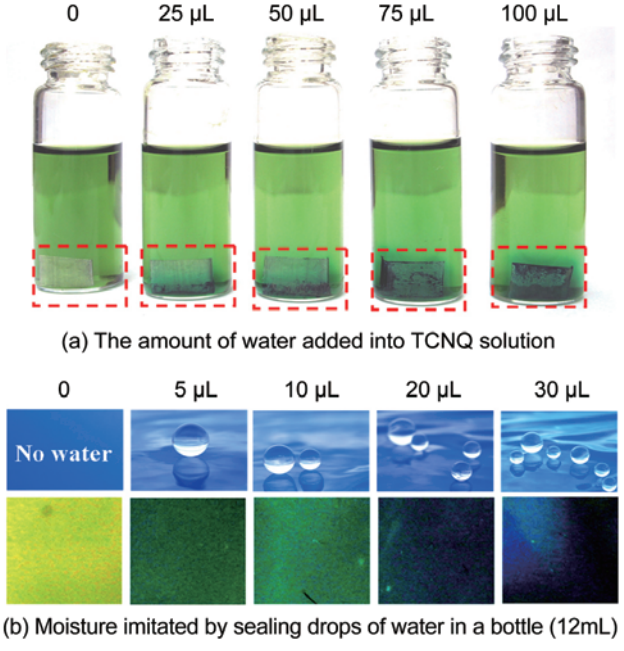

Figure 7 Fabrication of the new water and moisture indicator based on the reaction of Zn, TCNQ, and traces of water to afford $Zn[TCNQ]_2(H_2O)_2$; the color change is an efficient way of detecting the presence of water and moisture. All samples involve the same reaction time of 1 min

content (the simulated moisture was obtained by adding different numbers of drops of water into a hermetically sealed bottle as shown in Fig. 7(b) (the volume of the bottle was 12 mL and one drop of water was around 5 μL).

In summary, low-dimensional molecular crystallites of square columns and nanolamellae of $Zn[TCNQ]_2(H_2O)_2$ with large areas (from several mm^2 to 10–20 cm^2) have been synthesized by controlled addition of water. The square columns of $Zn[TCNQ]_2(H_2O)_2$ were identified as the kinetic product phase I, and the nanolamellae were the thermodynamic product phase II. Based on the accurate control of the synthesis of $Zn[TCNQ]_2(H_2O)_2$ by reaction between Zn and TCNQ induced by addition of water, i) the transformation mechanism from square columns to nanolamellae was clearly monitored, ii) the size of the micro and nanometer sized crystals of $Zn[TCNQ]_2(H_2O)_2$ can be finely tuned, iii) and a new moisture and water indicator has been developed. Devices based on an individual square column or nanolamella demonstrated the typical semiconductor behavior of the single crystalline products. This simple method for the large scale synthesis, the ability to fine tune the size, and the typical semiconductor behavior of the low-dimensional molecular materials are attractive in terms of developing new materials for molecular electronics and nanoelectronics. The new water or moisture indicator can be used for the inspection of water and moisture, such as monitoring the presence of traces of water, leak hunting or moisture monitoring.

Experimental

The zinc plates were successively cleaned with pure water, ethanol, acetone, dilute HCl, and pure water. After cleaning, the zinc plates were immersed into a TCNQ/acetonitrile solution, and then drops of water were carefully added. Finally, the zinc plates were removed from the TCNQ solution and gently washed with acetonitrile to remove any excess TCNQ, followed by drying under a stream of N_2.

The $Zn[TCNQ]_2(H_2O)_2$ products were characterized by UV-visible spectroscopy (U3010), FT-IR (PE2000), XPS (ESCALab220I-XL), X-ray diffraction (XRD) (D/max2500), scanning electron microscope (SEM) (Hitachi S-4300 SE), and TEM (JEOL 2010). A Keithley 4200 SCS Semiconductor Characterization System was used to measure the current–voltage characteristics of the nanorods.

Acknowledgements

The authors acknowledge the financial support from the National Natural Science Foundation of China (Nos. 20721061, 50725311), the Ministry of Science and Technology of China (2006CB806200, 2006CB932100) and the Chinese Academy of Sciences.

Electronic Supplementary Material: Supplementary material is available in the online version of this article at http://dx.doi.org/10.1007/s12274-009-9084-x and is accessible free of charge. It contains further experimental details, information about the fabrication of low dimensional molecular crystals, including typical SEM images and the corresponding energy-dispersive X-ray (EDX) traces of the columns and lamellae, XPS data for the sub-micro columns, TGA traces for the square micro columns, the UV-visible spectrum of the square columns, large area images of square columns and nanolamellae, and the mechanism of formation of square columns of $Zn[TCNQ]_2(H_2O)_2$.

References

[1] Acker, D. S.; Harder, R. J.; Hertler, W. R.; Mahler, W.; Melby, L. R.; Benson, R. E.; Mochel, W. E. 7,7,8,8-Tetracyanoquinodimethane and its electrically conducting anion-radical derivatives. *J. Am. Chem. Soc.* **1960**, *82*, 6408–6409.

[2] Wheland, R. C.; Gillson, J. L. Synthesis of electrically conductive organic solids. *J. Am. Chem. Soc.* **1976**, *98*, 3916–3925.

[3] Kathirgamanathan, P.; Rosseinsky, D. R. Electrocrystallized metal-tetracyanoquinodimethane salts with high electrical-conductivity. *J. Chem. Soc., Chem. Commun.* **1980**, *17*, 839–840.

[4] Bolinger, C. M.; Darkwa, J.; Gammie, G.; Gammon, S. D.; Lyding, J. W.; Rauchfuss, T. B.; Wilson, S. R. Synthesis, structure, and electrical properties of

[(MeCp)$_5$V$_5$S$_6$][(TCNQ)$_2$]. *Organomet.* **1986**, *5,* 2386–2388.

[5] Kulys, J.; Drungiliene, A. Electrocatalytic oxidation of ascorbic acid at chemically modified electrodes. *Electroanal.* **1991**, *3,* 209–214.

[6] Murthy, A. S. N.; Anita, G. R. L. NADH sensor with electrochemically modified TCNQ electrode. *Anal. Chim. Acta* **1994**, *289,* 43–46.

[7] Wooster, T. J.; Bond, A. M.; Honeychurch, M. J. An analogy of an ion-selective electrode sensor based on the voltammetry of microcrystals of tetracyanoquinodimethane or tetrathiafulvalene adhered to an electrode surface. *Anal. Chem.* **2003**, *75*, 586–592.

[8] Wooster, T. J.; Bond, A. M. Ion selectivity obtained under voltammetric conditions when a TCNQ chemically modified electrode is presented with aqueous solutions containing tetraalkylammonium cations. *Analyst* **2003**, *128***,** 1386–1390.

[9] Okamoto, T.; Kozaki, M.; Doe, M.; Uchida, M.; Wang, G.; Okada, K. 1,4-Benzoxazino[2,3-b]phenoxazine and its sulfur analogues: Synthesis, properties, and application to organic light-emitting diodes. *Chem. Mater.* **2005**, *17*, 5504–5511.

[10] Mueller, R.; Jonge, S. D.; Myny, K.; Wouters, D. J.; Genoe, J.; Heremans, P. Organic CuTCNQ non-volatile memories for integration in the CMOS backend-of-line: Preparation from gas/solid reaction and downscaling to an area of 0.25 μm^2. *Solid State Electron.* **2006**, *50*, 601–605.

[11] Heintz, R. A.; Zhao, H.; Ouyang, X.; Grandinetti, G.; Cowen, J.; Dunbar, K. R. New insight into the nature of Cu(TCNQ): Solution routes to two distinct polymorphs and their relationship to crystalline films that display bistable switching behavior. *Inorg. Chem*. **1999**, *38*, 144–156.

[12] Neufeld, A. K.; Madsen, I.; Bond, A. M.; Hogan, C. F. Phase, morphology, and particle size changes associated with the solid–solid electrochemical interconversion of TCNQ and semiconducting CuTCNQ (TCNQ = tetracyanoquinodimethane). *Chem. Mater.* **2003**, *15*, 3573–2585.

[13] Neufeld, A. K.; O'Mullane, A. P.; Bond, A. M. Control of localized nanorod formation and patterns of semiconducting CuTCNQ phase I crystals by scanning electrochemical microscopy. *J. Am. Chem. Soc.* **2005**, *127*, 13846–13853.

[14] O'Mullane, A. P.; Neufeld, A. K.; Bond, A. M. Distinction of the two phases of CuTCNQ by scanning electrochemical microscopy. *Anal. Chem.* **2005**, *77*, 5447–5452.

[15] O'Mullane, A. P.; Neufeld, A. K.; Harris, A. R.; Bond, A. M. Electrocrystallization of phase I, CuTCNQ (TCNQ = 7,7,8,8-tetracyanoquinodimethane), on indium tin oxide and boron-doped diamond electrodes. *Langmuir* **2006**, *22*, 10499–10505.

[16] Siedle, A. R.; Candela, G. A.; Finnegan, T. F. Transition-metal derivatives of the teracyanoquinodimethane ion, TCNQ^{2-}. *Inorg. Chim. Acta* **1979**, *35*, 125–130.

[17] Nafady, A.; O'Mullane, A. P.; Bond, A. M.; Neufeld, A. K. Morphology changes and mechanistic aspects of the electrochemically-induced reversible solid–solid transformation of microcrystalline TCNQ into Co[TCNQ]$_2$-based materials (TCNQ = 7,7,8,8-tetracyanoquino dimethane). *Chem. Mater.* **2006**, *18*, 4375–4384.

[18] Clerac, R.; O'Kane, S.; Cowen, J.; Ouyang, X.; Heintz, R.; Zhao, H.; Bazile, M. J.; Dunbar, Jr. K. R. Glassy magnets composed of metals coordinated to 7,7,8,8-tetracyanoq uinodimethane: M(TCNQ)$_2$ (M = Mn, Fe, Co, Ni). *Chem. Mater.* **2003**, *15*, 1840–1850.

[19] Nafady, A.; Bond, A. M.; Bilyk, M. A.; Harris, A. R.; Bhatt, A. I.; O'Mullane, A. P.; Marco, R. D. Tuning the electrocrystallization parameters of semiconducting Co[TCNQ]$_2$-based materials to yield either single nanowires or crystalline thin films. *J. Am. Chem. Soc.* **2007**, *129*, 2369–2382.

[20] Goh, S. H.; Lee, S. Y.; Zhou, X.; Tan, K. L. X-ray photoelectron spectroscopic studies of interactions between poly(4-vinylpyridine) and poly(styrenesulfonate) salts. *Macromolecules* **1998**, *31*, 4260–4264.

[21] Potember, R. S.; Poehler, T. O.; Cowan, D. O.; Carter, F. L.; Brant, P. I. In *Molecular Electronic Devices*; Carter, F. L., Eds.; Marcel Dekker: New York, 1982.

[22] Ikemoto, I.; Thomas, J. M.; Kuroda, H. X-ray photoelectron spectra of copper-tetracyanoquinodimethane complexes. *Bull. Chem. Soc. Jpn.* **1973**, *46*, 2237–2238.

[23] Khatkale, K. S.; Devlin, J. P. The vibrational and electronic spectra of the mono-, di-, and trianon salts of TCNQ. *J. Chem. Phys.* **1979**, *70*, 1851–1859.

[24] Zhao, H.; Heintz, R. A.; Ouyang, X.; Dunbar, K. R.; Campana, C. F.; Rogers, R. D. Spectroscopic, thermal,

and magnetic properties of metal/TCNQ network polymers with extensive supramolecular interactions between layers. *Chem. Mater*. **1999**, *11*, 736–746.

[25] Melby, L. R.; Harder, R. J.; Hertler, W. R.; Mahler, W.; Benson R. E. Substituted quinodimethans, II. Anion-radical derivatives and complexes of 7,7,8,8-tetracyano quinodimethan. *J. Am. Chem. Soc.* **1962**, *84*, 3374–3387.

[26] Jeanmaire, D. L.; van Duyne, R. P. Resonance Raman spectroelectrochemistry. 2. Scattering spectroscopy accompanying excitation of the lowest $^2B_{1u}$ excited state of the tetracyanoquinodimethane anion radical. *J. Am. Chem. Soc.* **1976**, *98*, 4029–4033.

[27] Gong, J. P.; Osada, Y. Preparation of polymeric metal-tetracyanoquinodimethane film and its bistable switching. *Appl. Phys. Lett.* **1992**, *61*, 2787–2789.

[28] Liu, S.; Liu, Y.; Wu, P.; Zhu, D. Multifaceted study of CuTCNQ thin-film materials. Fabrication, morphology, and spectral and electrical switching properties. *Chem. Mater.* **1996**, *8*, 2779–2787.

[29] Liu, Y.; Ji, Z.; Tang, Q.; Jiang, L.; Li, H.; He, M.; Hu, W.; Zhang, D.; Jiang, L.; Wang, X.; Wang, C.; Liu, Y.; Zhu, D. Particle-size control and patterning of a charge-transfer complex for nanoelectronics. *Adv. Mater.* **2005**, *17*, 2953–2958.

[30] Tang, Q.; Li, H.; He, M.; Hu, W.; Liu, C.; Chen, K.; Wang, C.; Liu, Y.; Zhu, D. Low threshold voltage transistors based on individual single-crystalline submicrometer-sized ribbons of copper phthalocyanine. *Adv. Mater.* **2006**, *18***,** 65–68.

[31] Lampert, M. A.; Mark, P. *Current Injection in Solids*; Academic Press: New York and London, 1970.